A Distributed Reactive Power Sharing Approach in Microgrid with Improved Droop Control

Xinsheng Wang, Jiancheng Zhang, Mingli Zheng and Lingyu Ma

***Abstract*—Conventional droop control causes frequency and voltage deviations (from rated value) in inverter-intensive microgrid (MG), and the reactive power sharing cannot be obtained when the communication structure of MG or load changes suddenly. Compared with centralized control and droop control scheme, distributed hierarchical control structure of MG can overcome the limitation of communication and realize the reactive power sharing. In this paper, the improved droop control is adopted, which is based on the hierarchical control structure. The hierarchical control structure consists of zero-level control, primary control and proposed secondary control. Firstly, the secondary controller is modeled, and the MG system composed of distributed generators (DGs) is considered as a multi-agent system. The secondary controller can make up for the shortcomings of the droop controller and adjust the frequency and voltage to their rated values. Secondly, the reference voltage and frequency of the zero-level control are calculated, combined with primary control. The zero-level control and primary control can make the voltage and frequency of MG run stably and provide reference voltage for the inverter. Finally, the stability of the system is proved by the theory of multi-agent consistency. A simulation system is established in Matlab/Simulink environment, and the results show the effectiveness of the proposed controller.**

***Index Terms*—microgrid; distributed generator; hierarchical control; consensus; reactive power sharing.**

I. Introduction

Microgrid (MG) is a distributed system, which is composed of several distributed generators (DGs), energy storage equipment and loads [1], [2]. It can operate in two modes, grid-connected mode and islanded mode [3]. Reasonable and effective control strategy is the basis of MG operation. Conventional droop control regulates voltage and frequency by power, and makes them stable when the system is disturbed [4]. No communication between the devices is required in MG with conventional droop control [5]-[7]. However, this control method is easy to be affected by the load change and disproportionate line impedance of MG, which often leads to the problem of dynamic performance [8]. In addition, the parallel operation of DG in MG will make the reactive power sharing unavailable [9], and the deviations of frequency and voltage from their rated values will also occur when MG is in switching topology or disturbed by load.

To make up for the deficiency of droop control, J. He proposed a MG control method without using droop control [10], A. Micallef proposed a reactive power sharing approach in droop-controlled MG [11]. These methods of using central controllers make the system of MG dependent on communication networks. In this way, there is a single fault point in the system, which makes the system unreliable. In order to avoid the use of central controller and reduce the dependence on communication network, a completely decentralized hierarchical control method is adopted to realize frequency adjustment and power optimization [12], [13]. Using this method, DGs do not communicate with each other, which makes the coordinated control of the system impossible. With the intention of making the networks of agents with switching topology control more flexible, a distributed control strategy is proposed in [14], which considers the DGs of MG as a multi-agent system. For instance, N. M. Dehkordi proposed a fully distributed cooperative control, which is based on the multi-agent consensus theory [15]. This method effectively controls the frequency and voltage. W. Liu proposed a distributed cooperative frequency control. This method considers MG composed of DGs as a multi-agent system considering communication constraints [16], and X. Wang presented a distributed finite-time cooperative control under switching topology [17]. However, using the above methods, the reactive power sharing cannot be obtained.

In practice, the DGs are widely distributed, and the distance between them is different. So the link impedances of DGs are not equal. To obtain the power sharing, the link impedances between DGs should be proportional. Z. Zhang [18] proposed a distributed cooperative control with coordinate rotational virtual impedance, which needs a leader in system and will fail when the leader fails. Y. Zhu [19] presented an enhanced optimization method with virtual impedance. Using this method, the reactive power sharing in MG is obtained. H. Xu [20] used a virtual capacitor method. However, the flexibility of the system using these two methods is poor under switching topology due to no communication between DGs. The methods mentioned above realize reactive power sharing, but each has its own shortcomings. Moreover, MG should work

This work was supported by the Natural Science Foundation of Shandong Province, P. R. China (No. ZR2017MEE053).

X. S. Wang, J. C. Zhang (corresponding author, e-mail: zhangjianchenghit@126.com), and M. L. Zheng are with the Department of Control Science and Engineering, Harbin Institute of Technology, No. 2 Culture West Road, Weihai, P. R. China.

L. Y. Ma is with the Department of Information Engineering, Shandong Management University, No. 3500 DingXiang Road, Jinan, P. R. China.

DOI: 10.17775/CSEEJPES.2019.00530

normally when the communication structure of MG changes, i.e., it is very important to improve the plug-and-play capability. So we will consider the reactive power sharing problem based on distributed cooperative algorithm under switching topology.

In this paper, distributed hierarchical control is used to obtain power sharing. Dual loop control is used as zero-level control. The primary control consists of droop control, and the secondary control is introduced to eliminate deviations and share active and reactive power. Be different form [21]-[23], the system does not require a leader, and transmits the voltage and measured power values as information between two DGs. The stability of the control strategy is proved by multi-agent theory. The proposed control method is verified in MATLAB/SIMULINK environment.

This paper is organized as follows. The proposed hierarchical control structure is modeled in Section II. The power sharing and stability of MG are demonstrated in Section III. The proposed control method is verified using MATLAB/SIMULINK in Section IV. The conclusion of this paper is in Section V.

II. Distributed Control Framework

To improve the reliability of MG, achieve the power sharing and compensate the deviations, this paper presents a distributed hierarchical control method. We will discuss it in detail next.

A. Primary Control

The conventional droop control is usually used as the primary control, which can stabilize the voltage and frequency of the system [24]. The structure diagram of DG based on inverter is shown in Fig. 1.

When the line impedance of MG is inductive, the frequency and voltage of each DG will be synchronized to the rated values by conventional droop control. Once the sum of the nominal power is not equal to the one of power at the output of inverter, the voltage and frequency of each DG will deviate from the reference values respectively. According to the droop characteristics of P/ω and Q/e, the active and reactive power sharing could be achieved if the voltage and frequency are synchronized.

$$\begin{cases} \omega_i^* = \omega_{rated} - m_i P_i \\ e_i^* = e_{rated} - n_i Q_i \end{cases} \tag{1}$$

The conventional droop controllers' theory is (1), where ω_i^* is the reference angular frequency output by the primary controller. [21], e_i^* is the reference voltage value output by the primary controller, P_i and Q_i are the measured active and reactive power of ith DG, m_i and n_i are the droop coefficients, ω_{rated} and e_{rated} are rated voltage and rated frequency respectively.

In practice, the DGs are widely distributed, and their distance from the load is different. So the link impedances of DGs are not equal. Although the conventional droop control can stabilize the frequency and voltage of MG, the deviations of frequency and voltage from their rated values will occur when the system operates stably. As a result, the active and reactive power sharing will not be obtained under complex line impedance or unbalanced loads. At this time, it is necessary to introduce secondary control.

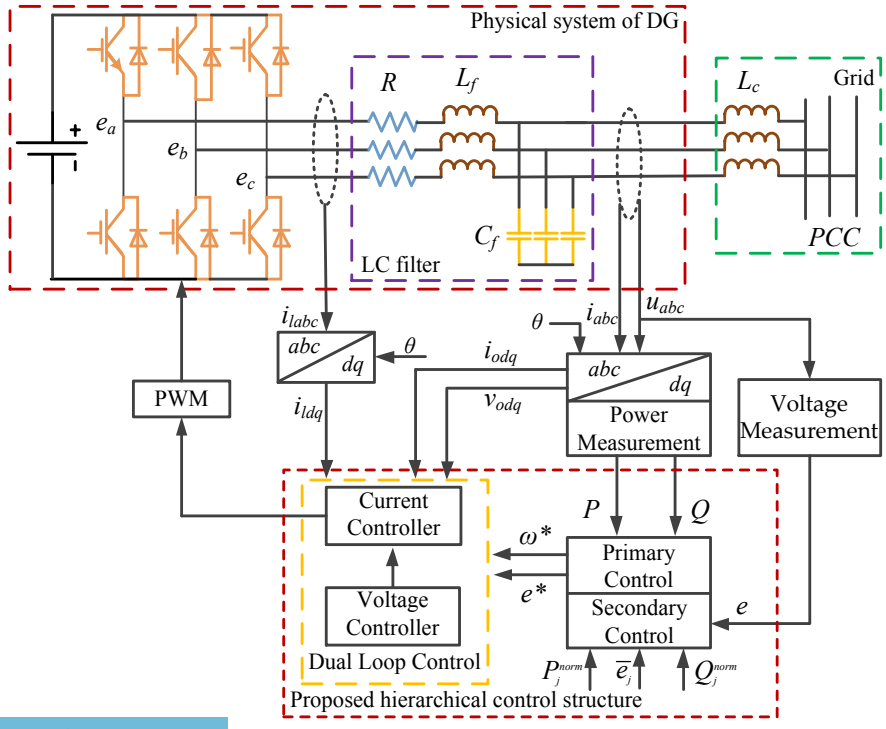

Fig. 1. Internal structure diagram of a DG

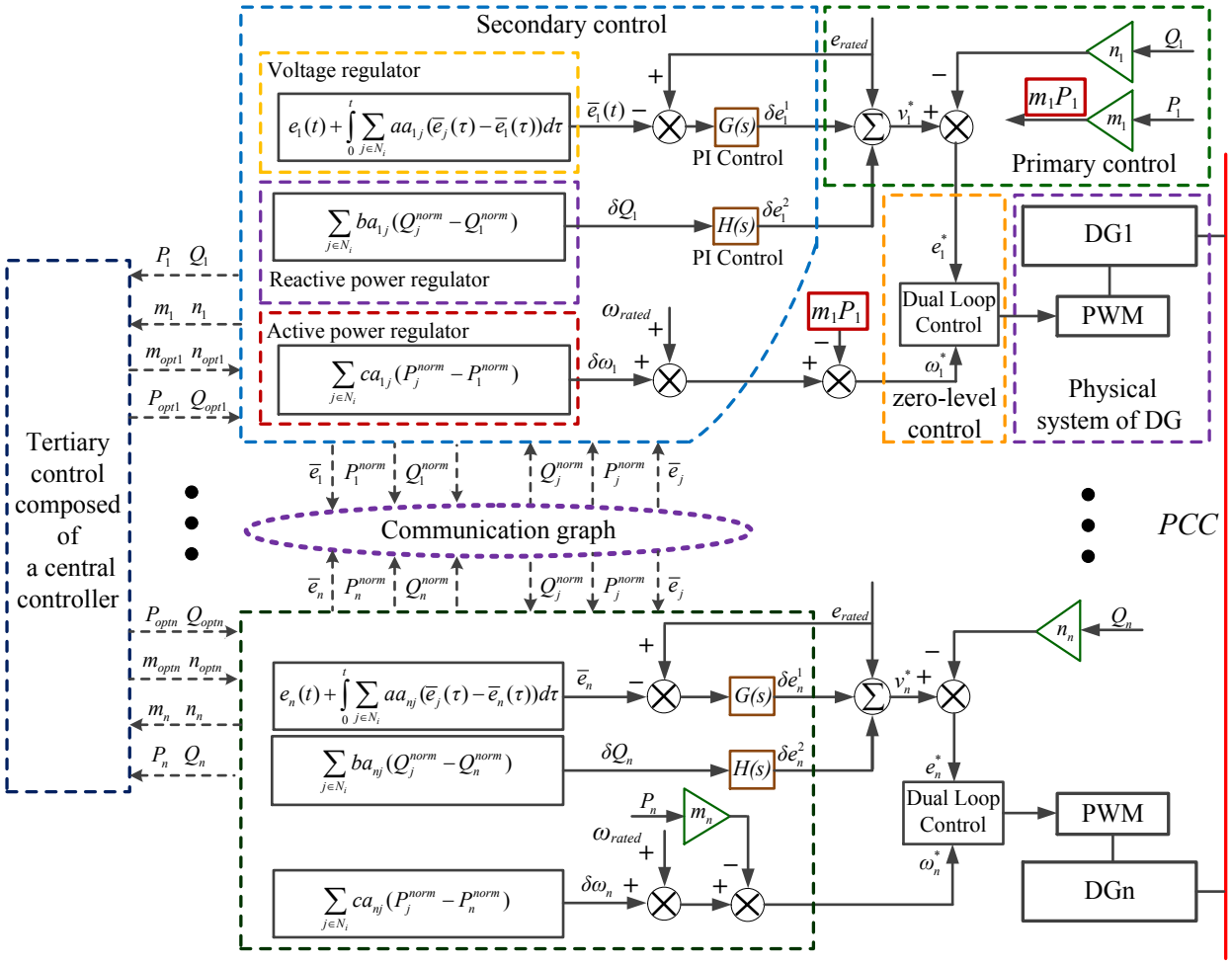

Fig. 2. The proposed structure of distributed hierarchical control

B. Secondary Control

To eliminate the deviations of frequency and voltage from their rated values and obtain power sharing, the secondary control is indispensable. Fig. 2 is the proposed distributed hierarchical control framework for MG.

Inspired by the properties of multi-agent consistency, this paper establishes a secondary controller, as shown in Fig. 2. The controller consists of three parts: voltage part, reactive power part and active power part.

The voltage regulator generates correction δe_i^1, and the reactive power regulator generates correction δe_i^2. These two corrections eliminate the deviation of voltage from rated voltage. The equation is shown in (2).

$$v_i^*(t) = e_{rated} + \delta e_i^1 + \delta e_i^2 \tag{2}$$

The MG system composed of DGs is considered as a multi-agent system (MAS). In MAS, the agent interacts with adjacent agents through distributed communication systems, and then judges its own operation status. It adjusts the output according to these information, so that it is identical with the target features of adjacent agents. Overall consistency is achieved finally. Using this property, the output of the voltage estimator is

$$\overline{e}_i(t) = e_i(t) + \int_0^t \sum_{j\in N_i} aa_{ij}(\overline{e}_j(\tau) - \overline{e}_i(\tau))d\tau \tag{3}$$

where a_{ij} represents the communication weight，a is a designed parameter. The function of voltage estimator is to estimate the average voltage value of MG.

The deviation between predicted voltage and rated voltage is fed back to PI controller $G(s)$, and then the PI controller produces the first correction term δe_i^1 after eliminating static error. Through the function of voltage regulator, the average value will converge to the nominal voltage of DG, but there may be a deviation between the voltage value of DG and the rated voltage value. So it is necessary to introduce another correction term δe_i^2. After the adjustment of secondary control, the average voltage of MG and the voltage of DG are adjusted towards the rated value. Similar to the voltage regulator, the deviation generated by the reactive power regulator is shown as

$$\delta Q_i = \sum_{j\in N_i} ba_{ij}(Q_j^{norm} - Q_i^{norm}) \tag{4}$$

where $Q_i^{norm} = Q_i / Q_i^{rated}$, b is a designed parameter. The purpose of this regulator is to make the nominal reactive power of each DG tend to be equal, so as to obtain the reactive power sharing.

Then the deviation δQ_i is fed back to PI controller *H(s)*, and the PI controller produces another correction term δe_i^2 after eliminating static error.

The function of the active power regulator is to adjust the frequency of DG to the rated value, and make the nominal active power of each DG tend to be equal, so as to obtain the active power sharing. The deviation $\delta\omega_i$ generated by the active power regulator based on MAS is shown as

$$\delta\omega_i = \sum_{j\in N_i} ca_{ij}(P_j^{norm} - P_i^{norm}) \tag{5}$$

where $P_i^{norm} = P_i / P_i^{rated}$, c is a designed parameter. By the above equations the angular frequency set-point is

$$\omega_i^*(t) = \omega_{rated} + \delta\omega_i(t) - m_i P_i \tag{6}$$

So the voltage setting is

$$E_i^* = e_i^* \sqrt{2}\sin(\theta_i) \tag{7}$$

The voltage set-points and phase angle are as follows:

$$e_i^* = e_{rated} + \delta e_i^1 + \delta e_i^2 - n_i Q_i \tag{8}$$

$$\theta_i = \int_0^t \omega_i^*(t)d\tau \tag{9}$$

where δe_i^1 and δe_i^2 are described in detail in the next section.

When the primary controller is used to adjust the voltage, the voltage is usually transferred to d / q coordinate system through coordinate transformation. The controller adjusts the component of the output voltage on the d-axis to make it equal to the voltage set-point [21]. Therefore, the second equation of (1) can be written as

$$\begin{cases} U_{drefi} = e_{rated} - n_i Q_i \\ U_{qrefi} = 0 \end{cases} \tag{10}$$

where U_{drefi} and U_{qrefi} are the d and q axis components of e_i^*, respectively.

From the above equations, we can see that the function of the voltage regulator and reactive power regulator is to eliminate the voltage deviation and maintain the voltage amplitude at the rated value, so as to realize reactive power sharing. Active power regulator maintains the frequency at the rated value, and eliminates the active power deviation from adjacent DG by adjusting the set-points of the phase angle to achieve active power sharing.

C. Dual loop control

The dual loop controller consists of a voltage loop controller and a current loop controller. The outer loop is the voltage loop and the inner loop is the current loop. The dual loop controller and the droop controller work together to stabilize the voltage and frequency of DG. The location of this controller in the system is shown in Fig. 2. The model of the outer loop is shown in (11) [21],

$$\begin{cases} i_{ld}^* = Fi_{od} - \omega_{ref} C_f v_{oq} + K_{PV}(U_{dref} - v_{od}) \\ \quad + K_{IV}\int (U_{dref} - v_{od})dt \\ i_{lq}^* = Fi_{oq} + \omega_{ref} C_f v_{od} + K_{PV}(U_{qref} - v_{oq}) \\ \quad + K_{IV}\int (U_{qref} - v_{oq})dt \end{cases} \tag{11}$$

where K_{PV} is the gain coefficient and K_{IV} is integral coefficient. C_f is the capacitance of the LC filter. The model of the inner loop is shown in (12):

$$\begin{cases} v_{PWMd} = -\omega_{ref} L_f i_{lq} + K_{PI}(i_{ld}^* - i_{ld}) + K_{II}\int (i_{ld}^* - i_{ld})dt \\ v_{PWMq} = \omega_{ref} L_f i_{ld} + K_{PI}(i_{lq}^* - i_{lq}) + K_{II}\int (i_{lq}^* - i_{lq})dt \end{cases} \tag{12}$$

where K_{PI} is the gain coefficient and K_{II} is integral coefficient. L_f is the inductor of the LC filter.

Hierarchical control also includes tertiary control used as scheduling layer, shown in Fig. 2. Tertiary layer composed of a central controller usually controls the power flow, and is often used when considering the cost of generating electricity, which is not the focus of this article.

III. Steady-State Analysis

The primary control and the secondary control operate with different timeframes, thus the controller design of the two levels is decoupled. The correction terms δe_i^1 and δe_i^2 are written as

$$\delta e_i^1 = G(e_{rated} - \bar{e}_i) \tag{13}$$

$$\delta e_i^2 = H \cdot \delta Q_i \tag{14}$$

Considering the whole MG, the equations (13) and (14) can be written in matrix form, expressed as

$$\boldsymbol{\delta e}^1 = \boldsymbol{\delta e}_0^1 + (\boldsymbol{G}_P + \boldsymbol{G}_I(t - t_0))(\boldsymbol{e}_{rated} - \bar{\boldsymbol{e}}) \tag{15}$$

$$\boldsymbol{\delta e}^2 = \boldsymbol{\delta e}_0^2 + (\boldsymbol{H}_p + \boldsymbol{H}_I(t - t_0))\boldsymbol{\delta Q} \tag{16}$$

where $\boldsymbol{G_I}$ and $\boldsymbol{G_P}$ are the diagonal matrices carrying the integral and proportional gains of the voltage-regulator matrix $\boldsymbol{G}$ such that $\boldsymbol{G}_P + \boldsymbol{G}_I / s = \boldsymbol{G}$. $\boldsymbol{H_I}$ and $\boldsymbol{H_P}$ are similar to $\boldsymbol{G_I}$ and $\boldsymbol{G_P}$ respectively. $\bar{\boldsymbol{e}} = [\bar{e}_1, \bar{e}_2, ..., \bar{e}_n]^{\mathrm{T}}$ denotes the voltage estimation vector, $\boldsymbol{\delta e_0^1}$ and $\boldsymbol{\delta e_0^2}$ are the initial values of integrators $\boldsymbol{G_I}$ and $\boldsymbol{H_I}$ at $t = t_0$, respectively. $\boldsymbol{\delta Q} = [\delta Q_1, \delta Q_2, ..., \delta Q_n]^{\mathrm{T}}$, all elements of $\boldsymbol{e}_{rated} \in R^{N\times 1}$ are made up of e_{rated}.

Next, we take the differential on both sides of (3), there is

$$\begin{aligned} \dot{\bar{e}}_i(t) &= \dot{e}_i(t) + \sum_{j\in N_i} a_{ij}(\bar{e}_j(t) - \bar{e}_i(t)) \\ &= \dot{e}_i(t) + \sum_{j\in N_i} a_{ij}\bar{e}_j(t) - d_i^{in}\bar{e}_i \end{aligned} \tag{17}$$

considering the whole MG, the equation (17) can be written in matrix form, expressed as

$$\begin{aligned} \dot{\bar{\boldsymbol{E}}} &= \dot{\boldsymbol{E}} + \boldsymbol{A_G}\bar{\boldsymbol{E}} - \boldsymbol{D}_G^{in}\bar{\boldsymbol{E}} \\ &= \dot{\boldsymbol{E}} + (\boldsymbol{A_G} - \boldsymbol{D}_G^{in})\bar{\boldsymbol{E}} \\ &= \dot{\boldsymbol{E}} - \boldsymbol{L}\bar{\boldsymbol{E}} \end{aligned} \tag{18}$$

Therefore the above equation is expressed in frequency domain as

$$\bar{\boldsymbol{E}} = s(s\boldsymbol{I_N} + \boldsymbol{L})^{-1}\boldsymbol{E} \tag{19}$$

where $\boldsymbol{I_N} \in \boldsymbol{R}^{N\times N}$, $\boldsymbol{e}=[e_1, e_2, \ldots, e_n]^T$ is the voltage measurement vector, $\boldsymbol{E}$ and $\bar{\boldsymbol{E}}$ are the Laplace transforms of $\boldsymbol{e}$ and $\bar{\boldsymbol{e}}$, respectively. $\boldsymbol{A_G}$ represents the communication weight matrix,

$\boldsymbol{D}_G^{in} = diag\{d_i^{in}\}$ is a diagonal matrix with $d_i^{in} = \sum_{j \in N_i} a_{ij}$, $\boldsymbol{L}$ is a Laplacian matrix in Graph Theory.

According to reference [14], a communication structure with a spanning tree has the following relationships,

$$\lim_{s \to 0} s(s\boldsymbol{I}_N + \boldsymbol{L})^{-1} = \boldsymbol{M}$$

where $\boldsymbol{M} \in \boldsymbol{R}^{N \times N}$ is a matrix in which all elements are $1/N$. Using this property and the final value theorem, equation (3) can be written as

$$\lim_{t \to \infty} \bar{\boldsymbol{e}}(t) = \lim_{s \to 0} s\bar{\boldsymbol{E}} = \lim_{s \to 0} s(s\boldsymbol{I}_N + \boldsymbol{L})^{-1}(s\boldsymbol{E})$$
$$= \lim_{s \to 0} s(s\boldsymbol{I}_N + \boldsymbol{L})^{-1} \times \lim_{s \to 0}(s\boldsymbol{E}) = \boldsymbol{M} \times \lim_{t \to \infty}(\boldsymbol{e}) = \langle \boldsymbol{e}^{ss} \rangle \boldsymbol{1}$$

where $\boldsymbol{e}^{ss} \in R^{N \times 1}$ is the steady state value of vector $\boldsymbol{e}$. $\langle \boldsymbol{e} \rangle$ is the average of all elements of vector $\boldsymbol{e}$. All elements of $\boldsymbol{1} \in R^{N \times 1}$ are 1. For the whole system, (4) can be written in matrix form, expressed as

$$\boldsymbol{\delta Q} = -b\boldsymbol{L}\boldsymbol{Q}^{norm} \tag{20}$$

When the system is stable, (15) and (16) can be written as (21) and (22) through the above derivation, respectively. There are

$$\boldsymbol{\delta e}^{1} = \boldsymbol{\delta e}_0^{1} + (\boldsymbol{G}_P + \boldsymbol{G}_I(t - t_0))(\boldsymbol{e}_{rated} - \boldsymbol{M}\boldsymbol{e}^{ss}) \tag{21}$$

$$\boldsymbol{\delta e}^{2} = \boldsymbol{\delta e}_0^{2} + (\boldsymbol{H}_p + \boldsymbol{H}_I(t - t_0))(-b\boldsymbol{L}\boldsymbol{Q}^{norm,ss}) \tag{22}$$

where $\boldsymbol{Q}^{norm,ss}$ is the stable state value of vector $\boldsymbol{Q}^{norm}$, $\boldsymbol{Q}^{norm} = [\frac{Q_1}{Q_1^{rated}}, \frac{Q_2}{Q_2^{rated}}, ..., \frac{Q_n}{Q_n^{rated}}]^{\mathrm{T}}$. As shown in Fig. 2, the reference voltage value output by the proposed controller in stable state can be expressed as

$$\boldsymbol{e}^{*ss} = \boldsymbol{e}_{rated} + \boldsymbol{\delta e}^{1} + \boldsymbol{\delta e}^{2} - \boldsymbol{N}\boldsymbol{Q}^{ss}$$
$$= \boldsymbol{e}_{rated} + \boldsymbol{\delta e}_0^{1} + \boldsymbol{\delta e}_0^{2} + \boldsymbol{G}_P(\boldsymbol{e}_{rated} - \langle \boldsymbol{e}^{ss} \rangle \boldsymbol{1}) - b\boldsymbol{H}_P\boldsymbol{L}\boldsymbol{Q}^{norm,ss} \tag{23}$$
$$+(\boldsymbol{G}_I(\boldsymbol{e}_{rated} - \langle \boldsymbol{e}^{ss} \rangle \boldsymbol{1}) - b\boldsymbol{H}_I\boldsymbol{L}\boldsymbol{Q}^{norm,ss})(t - t_0) - \boldsymbol{N}\boldsymbol{Q}^{ss}$$

where $\boldsymbol{N} = diag\{n_i\}$, $\boldsymbol{Q}^{ss}$ and $\boldsymbol{e}^{*ss}$ is the steady-state value of $\boldsymbol{Q} = [Q_1, Q_2, ..., Q_n]^{\mathrm{T}}$ and $\boldsymbol{e}^{*} = [e_1^{*}, e_2^{*}, ..., e_n^{*}]^{\mathrm{T}}$, respectively. Equation (23) holds for all $t \geq t_0$. Therefore, the time-varying part in (23) is zero. There is

$$b^{-1}\boldsymbol{H}_I^{-1}\boldsymbol{G}_I(\boldsymbol{e}_{rated} - \langle \boldsymbol{e}^{ss} \rangle \boldsymbol{1}) = \boldsymbol{L}\boldsymbol{Q}^{norm,ss} \tag{24}$$

Multiplying (24) by $\boldsymbol{1}^{\boldsymbol{T}}$, (25) can be obtained.

$$\boldsymbol{1}^{T} b^{-1}\boldsymbol{H}_I^{-1}\boldsymbol{G}_I(\boldsymbol{e}_{rated} - \langle \boldsymbol{e}^{ss} \rangle \boldsymbol{1}) = \boldsymbol{1}^{T}\boldsymbol{L}\boldsymbol{Q}^{norm,ss} \tag{25}$$

Because the Laplace matrix satisfies the relation $\boldsymbol{1}^{T}\boldsymbol{L} = \boldsymbol{0}$ [14], and $\boldsymbol{1}^{T} b^{-1}\boldsymbol{H}_I^{-1}\boldsymbol{G}_I \neq \boldsymbol{0}$, there is

$$\boldsymbol{e}_{rated} = \langle \boldsymbol{e}^{ss} \rangle \boldsymbol{1} \tag{26}$$

So it can be obtained that,

$$e_{rated} = \langle \boldsymbol{e}^{ss} \rangle \tag{27}$$

It can be seen from (27) that the average voltage of all DGs in MG converges to the rated value under stable operation of MG. By substituting $\boldsymbol{e}_{rated} - \langle \boldsymbol{e}^{ss} \rangle \boldsymbol{1} = \boldsymbol{0}$ into (24),

$$\boldsymbol{L}\boldsymbol{Q}^{norm,ss} = \boldsymbol{0} \tag{28}$$

According to [25], the only nonzero solution of equation $\boldsymbol{L}\boldsymbol{x} = \boldsymbol{0}$ is $\boldsymbol{x} = k\boldsymbol{1}$, k is a real number. So according to (28), equation $\boldsymbol{Q}^{norm,ss} = k\boldsymbol{1}$ holds. This means that the nominal reactive power of each DG is equal to each other, i.e., the reactive power sharing is obtained.

Similar to the previous proof, (29) can be derived from (6).

$$c\boldsymbol{L}\boldsymbol{P}^{norm,ss} = \boldsymbol{0} \tag{29}$$

where $\boldsymbol{P}^{norm,ss}$ is the steady state value of $\boldsymbol{P}^{norm}$, $\boldsymbol{P}^{norm} = [\frac{P_1}{P_1^{rated}}, \frac{P_2}{P_2^{rated}}, ..., \frac{P_n}{P_n^{rated}}]^{\mathrm{T}}$, there is

$$\boldsymbol{P}^{norm,ss} = \xi\boldsymbol{1} \tag{30}$$

where ξ is a real number. This completes the proof.

IV. Simulation Validation

The proposed control method is verified in this section. The experimental setup is shown in Fig. 3, which consists of four DGs to form a MG system.

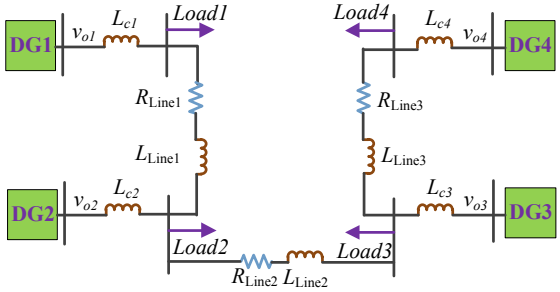

Fig. 3. Schematic of the MG physical system

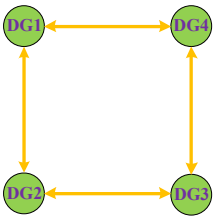

Fig. 4. Communication network

The communication structure is shown in Fig. 4. The line impedance parameters are shown in Table I, and the simulation parameters of each DG are listed in Table II given in the section TABLE.

TABLE I
LINE IMPEDANCE PARAMETERS OF MG

Symbol	Quantity	Value
Z_{Line1}	Line impedance	0.8+3.6*j*
Z_{Line2}	Line impedance	0.4+1.8*j*
Z_{Line3}	Line impedance	0.7+1.2*j*

The reference value of voltage is 120V, the reference value of angular frequency is 100π (rad/s), the filter inductance L_f is 1.8mH, the filter resistance R_f is 0.1Ω, and the filter capacitor C_f is 50μF. The remaining parameters are in Table II. Next, we verify the proposed method in two cases. The first case is to switch the load under the fixed communication structure. The second case is to verify the stability of the system under variable communication structure

A. Fixed Communication Structure

In order to compare with the conventional control method, only the primary controller works from 0s to 1s, and the proposed controller starts to work when t=1s. The total simulation time is 3 seconds. The calculation results of the two controllers are shown in Fig. 5.

As shown in Fig. 5, the conventional droop controller stabilizes the voltage and frequency, but they will deviate from their reference values. Moreover, the reactive power sharing is not obtained. Under the influence of the proposed hierarchical control, the frequency and voltage of each DG is regulated to the rated values respectively at about $t = 1.35s$. It can be seen from Fig.5(c) and (d) that $m_i p_i$ and $n_i q_i$ are equal to each other respectively, and the curves are completely coincident, i.e., the active and reactive power sharing are all obtained. As the voltage is synchronized to the reference value, the loads operate at rated voltage. So the total power emitted by each DG increases.

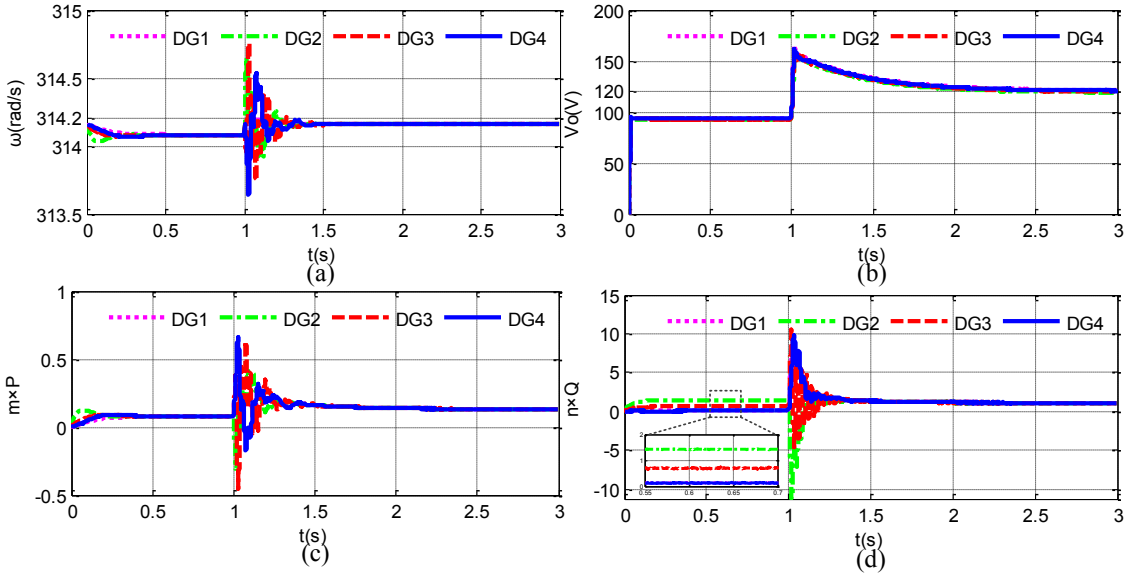

Fig. 5. Comparison of two control methods (a) frequency (b) voltage (c) active power ratios (d) reactive power ratios

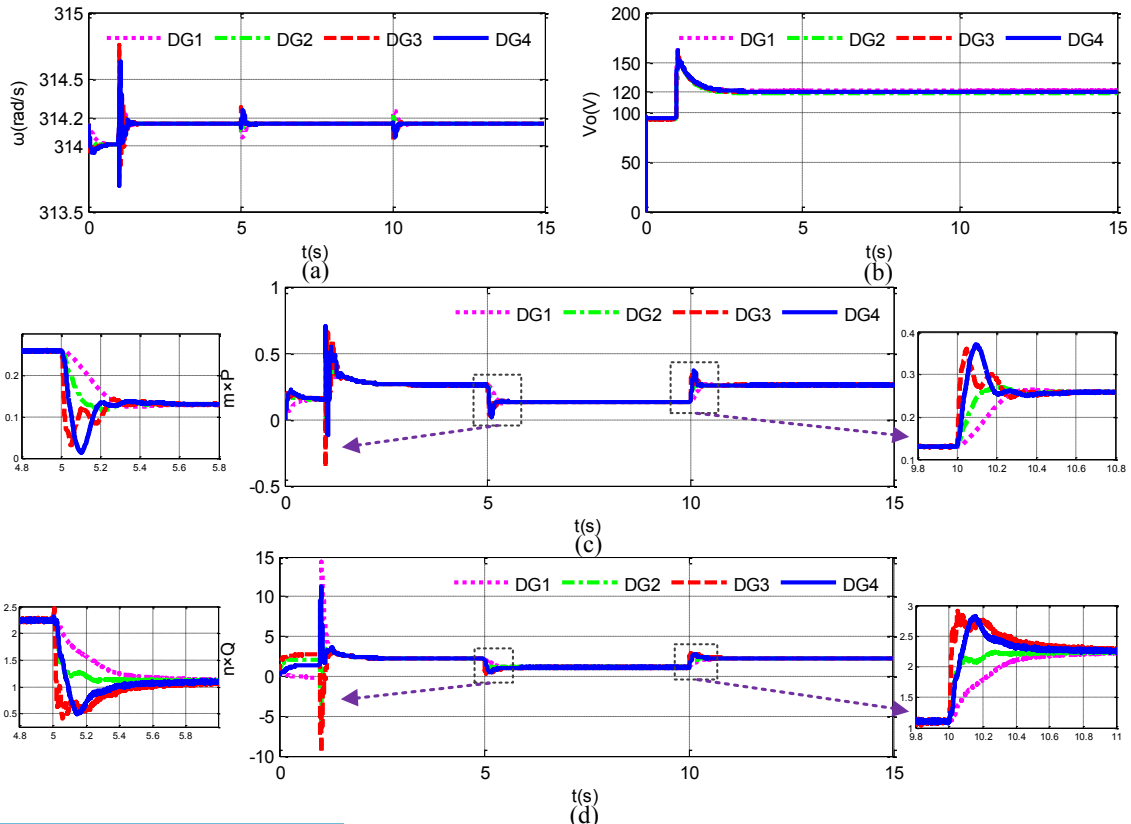

Fig. 6. Switching load under fixed communication structure. (a) frequency (b) voltage (c) active power ratios (d) reactive power ratios

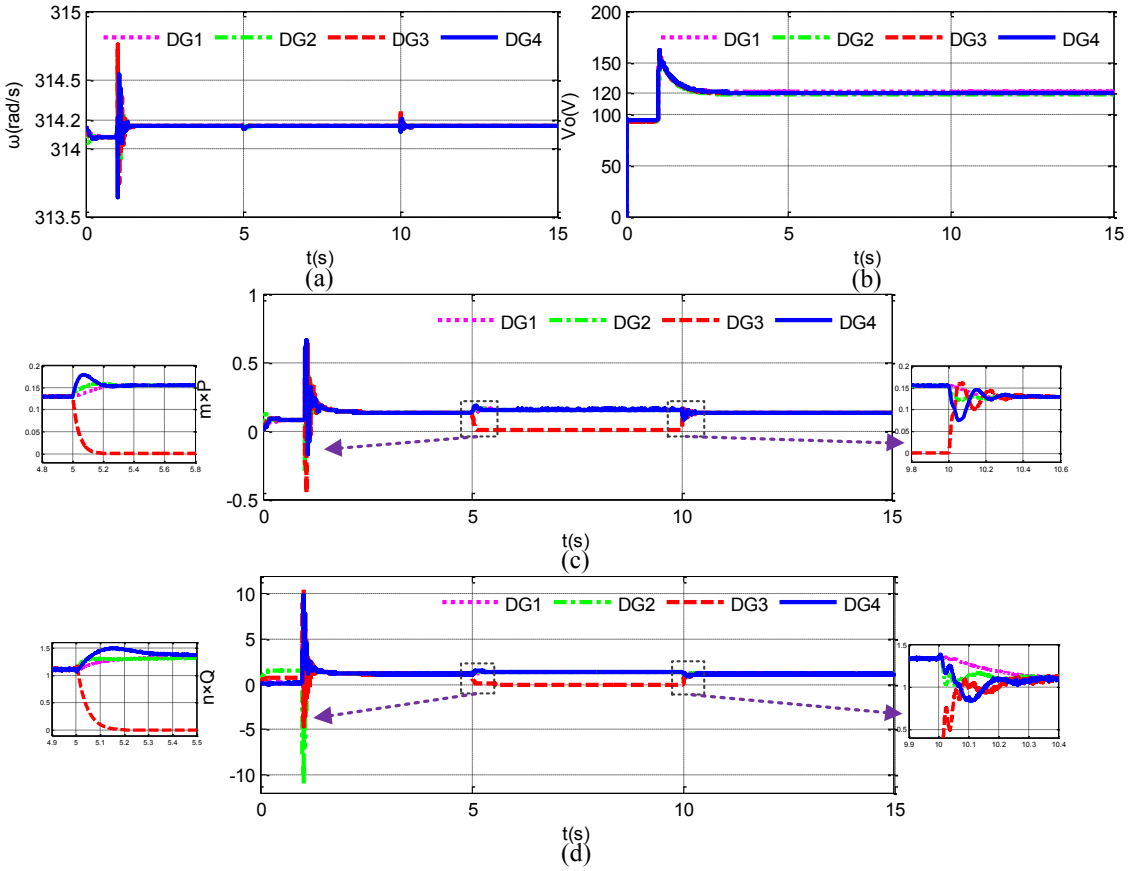

Fig. 8. Under switching communication structure. (a) frequency (b) voltage (c) active power ratios (d) reactive power ratios

The load of MG often changes suddenly in actual use. This will cause the power of each DG to change. When the load fluctuates, a good control method can make the system from the old balance point to the new balance point quickly. In the case of load change, the performance verification of the proposed controller is shown in Fig. 6. The proposed controller starts to work when t=1s. The load is disconnected from MG at $t = 5s$ and connected to MG at $t = 10s$. As seen, the frequency and voltage return to their reference values after slight fluctuation, and different power sharing points are achieved according to the variation of the load. This means that the method proposed in this paper is effective when the load fluctuates.

B. Variable Communication Structure

In this section, we verify the effectiveness of the method when the communication structure of the system changes. The communication structure of MG at t=0s is shown in Fig. 7. The proposed controller starts to work when t=1s. We assume that DG3 is disconnected from MG at $t = 5s$ and connected to MG at $t = 10s$ .Or DG3 is broken when $t = 5s$, and resumed when $t = 10s$.

The links of every switching topology still form a connected graph, thus the control method will remain functional. The performance verification of the proposed controller is shown in Fig. 8.

It can be seen from Fig. 8 that the control strategy proposed makes the frequency and voltage stable at their respective rates when the topology is switching. The active and reactive powers of DG3 drop to zero at $t = 5$s , while the powers supplied by other DGs keep sharing. When the topology is switched back at $t = 10$s , the power sharing is again obtained after about 0.4s. Similar to DG3 disconnection from MG, if DG3 fails, the rest of MG can work normally. These good performances show that the control method can enhance the flexibility and scalability of MG and improve the quality of power supply. The above cases show the effectiveness of the proposed method in this paper.

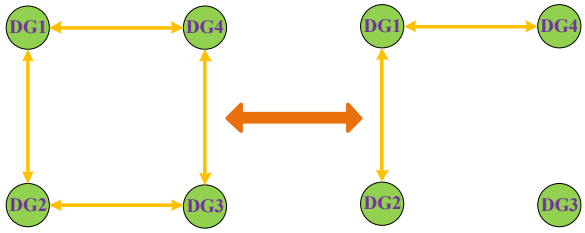

Fig. 7. Communication network configuration of switching topology

V. CONCLUSION

A distributed reactive power sharing approach in MG with improved droop control is proposed in this paper. This method adopts a hierarchical control structure, which not only retains the advantages of conventional droop control, but also makes up for its shortcomings. Based on the properties of multi-agent theory, the secondary controller is constructed. The stability and feasibility of the controller are proved by the final value theorem and multi-agent consistency. The proposed control strategy requires less amount of communication connection

and information exchange, which realizes the power sharing and adjusts voltage and frequency of MG to rated values respectively. This method saves the investment of communication equipment and circuits. At the same time, the proposed control strategy can enhance the flexibility and reliability of MG and improve the quality of power supply. The simulation results of fixed communication structure and variable communication structure show that the proposed control strategy can achieve accurate power sharing.

At present, there are many methods to realize reactive power sharing. But these methods have not been applied in practice. The method proposed in this paper provides a new way of thinking and research direction for large-scale practical application in the future. The application of the proposed method to practice will be the focus of the author's future research work.

VI. TABLE

TABLE II
SIMULATION PARAMETERS

SYMBOL	QUANTITY	DG1&DG2	DG3&DG4
U_{dc}	Dc-bus voltage	650 V	650 V
τ_{Qi}	Reactive power filter time constant	0.04 s	0.04 s
τ_{Pi}	Active filter time constant	0.04 s	0.04 s
R_c	Output end resistance	0.12&0.03 Ω	0.06&0.09 Ω
L_c	Output end inductance	1.4&0.35 mH	0.7&1.05 mH
n_i	Reactive droop coefficient	0.01 V/Var	0.02 V/Var
m_i	Active droop coefficient	4×10^{-4} rad/(s×W)	8×10^{-4} rad/(s×W)
Q	Reactive power load	0&200 Var	0&300 Var
P	Active power load	0&600 W	0&400 W
P^{rated}	Rated active power	800 W	400 W
Q^{rated}	Rated reactive power	600 Var	300 Var
k_{PQ}	$G_i(s)$ proportional term	0.01	0.01
k_{iQ}	$G_i(s)$ integral term	3	3
k_{pv}	$H_i(s)$ proportional term	0.005	0.005
k_{iv}	$H_i(s)$ integral term	2	2
a	Designed parameter	1.5	1.5
b	Designed parameter	30	30
c	Designed parameter	0.1	0.1

Note: the designed parameter $\boldsymbol{A_G}$ as follows:

$$\boldsymbol{A_G} = 1.5\times\begin{bmatrix} 0 & 1 & 0 & 1 \\ 1 & 0 & 1 & 0 \\ 0 & 1 & 0 & 1 \\ 1 & 0 & 1 & 0 \end{bmatrix}$$

REFERENCES

[1] C. Cai, S. Cheng, J. Bing, W. Dai, W. Min, and J. Zhang, "Optimal operation of microgrid composed of small hydropower and photovoltaic generation with energy storage based on multiple scenarios technique," in *International Conference on Electric Utility Deregulation & Restructuring & Power Technologies*, 2015.

[2] C. Dou, Z. Zhang, Y. Dong, and Y. Zheng, "MAS-based hierarchical distributed coordinate control strategy of virtual power source voltage in low-voltage microgrid," *IEEE Access,* vol. PP, no. 99, pp. 1-1, 2017.

[3] S. Parhizi, H. Lotfi, A. Khodaei, and S. Bahramirad, "State of the art in research on microgrids: a review," *IEEE Access,* vol. 3, pp. 890-925, 2015.

[4] Y. Zhu, F. Zhuo, F. Wang, and B. Liu, "Virtual impedance optimization method for microgrid reactive power sharing control," *Proceedings of the CSEE,* vol. 36, no. 17, 2016.

[5] H. Wang and L. I. Guoqing, "Control strategy of microgrid with different DG types," *Electric Power Automation Equipment,* vol. 32, no. 5, pp. 19-23, 2012.

[6] J. Huang, C. Jiang, and X. Rong, "A review on distributed energy resources and microgrid," *Renewable & Sustainable Energy Reviews,* vol. 12, no. 9, pp. 2472-2483, 2008.

[7] Y. Zheng, M. Chen, L. I. Chuang, X. U. Ruilin, and X. U. Xin, "A microgrid control strategy based on adaptive drooping coefficient adjustment," *Automation of Electric Power Systems,* vol. 37, no. 7, pp. 6-11, 2013.

[8] Y. Gao and Q. Ai, "A distributed coordinated economic droop control scheme for islanded AC microgrid considering communication system," *Electric Power Systems Research,* vol. 160, pp. 109-118, 2018.

[9] Z. Y. Yu, M. Lu, Z. N. Wang, and Y. G. Zhang, "A droop control strategy with impedance compensation for low voltage microgrid," *Applied Mechanics & Materials,* vol. 441, no. 8, pp. 245-248, 2014.

[10] J. He, C. Wang, Y. Pan, and B. Liang, "A simple decentralized islanding microgrid power sharing method without using droop control," *IEEE Transactions on Smart Grid,* vol. PP, no. 99, pp. 1-1, 2017.

[11] A. Micallef, M. Apap, C. S. Staines, and J. M. Guerrero, "Secondary control for reactive power sharing in droop-controlled islanded microgrids," in *IEEE International Symposium on Industrial Electronics*, 2012.

[12] H. Xin, Z. Rui, L. Zhang, W. Zhen, K. P. Wong, and W. Wei, "A decentralized hierarchical control structure and self-optimizing control strategy for f-p type DGs in islanded microgrids," *IEEE Transactions on Smart Grid,* vol. 7, no. 1, pp. 3-5, 2016.

[13] H. Xu, Z. Xing, L. Fang, R. Shi, C. Yu, and R. Cao, "A reactive power sharing strategy of VSG based on virtual capacitor algorithm," *IEEE Transactions on Industrial Electronics,* vol. 64, no. 9, pp. 7520-7531, 2017.

[14] Olfati-Saber, R. , and R. M. Murray, "Consensus problems in networks of agents with switching topology and time-delays," *IEEE Transactions on Automatic Control,* vol. 49, no. 9, pp. 1520-1533, 2004.

[15] N. M. Dehkordi, N. Sadati, and M. Hamzeh, "Fully distributed cooperative secondary frequency and voltage control of islanded microgrids," *IEEE Transactions on Energy Conversion,* vol. PP, no. 99, pp. 1-1, 2016.

[16] W. Liu, G. Wei, W. Sheng, X. Meng, and W. Chen, "Decentralized multi-agent system-based cooperative frequency control for autonomous microgrids with communication constraints," *IEEE Transactions on Sustainable Energy,* vol. 5, no. 2, pp. 446-456, 2017.

[17] X. Wang, H. Zhang, and C. Li, "Distributed finite-time cooperative control of droop-controlled microgrids under switching topology," *Iet Renewable Power Generation,* vol. 11, no. 5, pp. 707-714, 2017.

[18] Z. Zhang and L. Jiang, "Distributed cooperative control of microgrids with unbalance impedances," in *Control Conference*, 2016.

[19] Y. Zhu, Q. Fan, B. Liu, and W. Tao, "An enhanced virtual impedance optimization method for reactive power sharing in microgrids," *IEEE Transactions on Power Electronics,* vol. PP, no. 99, pp. 1-1, 2018.

[20] H. Xu, et al. "A reactive power sharing method based on virtual capacitor in islanding microgrid." *IEEE,* pp. 567-572, 2014.

[21] A. Bidram, A. Davoudi, F. L. Lewis, and J. M. Guerrero, "Distributed cooperative secondary control of microgrids using feedback linearization," *IEEE Transactions on Power Systems,* vol. 28, no. 3, pp. 3462-3470, 2013.

[22] F. Guo, C. Wen, J. Mao, and Y. D. Song, "Distributed secondary voltage and frequency restoration control of droop-controlled inverter-based microgrids," *IEEE Transactions on Industrial Electronics,* vol. 62, no. 7, pp. 4355-4364, 2015.

[23] N. M. Dehkordi, N. Sadati, and M. Hamzeh, "Fully distributed cooperative secondary frequency and voltage control of islanded microgrids," *IEEE Transactions on Energy Conversion,* vol. PP, no. 99, pp. 1-1, 2016.

[24] A. Bidram and A. Davoudi, "Hierarchical structure of microgrids control system," *IEEE Transactions on Smart Grid,* vol. 3, no. 4, pp. 1963-1976, 2012.
[25] Nasirian, Vahidreza , et al. , "Distributed cooperative control of DC microgrids," *IEEE Transactions on Power Electronics,* vol. 30, no. 4, pp. 2288-2303, 2015.

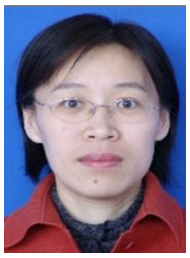

Xinsheng Wang received her B.S., M.S. and Ph.D. degrees from Harbin Institute of Technology, Harbin, China, in 1992, 1995 and 2002, respectively. She is now an associate professor of Control Science and Engineering in Harbin Institute of Technology, Weihai, China. Her research interests include robust and nonlinear control, power electronics system modeling and control.

Jiancheng Zhang received the B.S. degree from Hebei Polytechnic University, Tangshan, China, in 2010, the M.S. degree from Harbin Institute of Technology, Shenzhen, China, in 2013, and he is currently pursuing his Ph.D. degree in Harbin Institute of Technology, Harbin, China. His research interests include multi-agent cooperative control and grid-connected algorithm for microgrid.

Mingli Zheng received the B.S. degree from China Jiliang University, Hangzhou, China, in 2015, the M.S. degree from Harbin Institute of Technology, Weihai, China, in 2018, and she is now engaged in the research and development of automatic driving decision algorithm in Zhengzhou Yutong Bus Co., Ltd. Her research interests include multi-agent cooperative control and autonomous driving technologies.

Lingyu Ma received the B.S. degree from Shandong Jianzhu University, Jinan, China, in 2011, the M.S. degree from Harbin Institute of Technology, Shenzhen, China, in 2013. She is now a lecturer of Control Science and Engineering in Shandong Management University, Jinan, China. Her research interests include robust and nonlinear control, development and application of embedded system.